# Catadioptric Projectors

Yuanyuan Ding[1] Jing Xiao[2] Kar-Han Tan[3] Jingyi Yu[1]
[1]University of Delaware, Newark, DE, USA {ding,yu}@eecis.udel.edu
[2]Epson Research and Development Inc, San Jose, CA 95131, USA xiaoj@erd.epson.com
[3]Hewlett-Packard Company, Palo Alto, CA 94304, USA karhan.tan@hp.com

## Abstract

*We present a catadioptric projector analogous to a catadioptric camera by combining a commodity digital projector with additional optical units. We show that, by using specially shaped reflectors/refractors, catadioptric projectors can offer an unprecedented level of flexibility in aspect ratio, size, and field of view. We also present efficient algorithms to reduce projection artifacts in catadioptric projectors, such as distortions, scattering, and defocusing. Instead of recovering the reflector/refractor geometry, our approach directly models the light transport between the projector and the viewpoint using the light transport matrix (LTM). We show how to efficiently approximate the pseudo inverse of the LTM and apply it to find the optimal input image that produces least projection distortions. Furthermore, we present a projection defocus analysis for reflector and thin refractor based catadioptric projectors. We show that defocus blur can be interpreted as spatially-varying Gaussian blurs on the input image. We then measure the kernels directly from the LTM and apply deconvolution to optimize the input image. We demonstrate the practical uses of catadioptric projectors in panoramic and omni-directional projections. Our new system achieves much wider field-of-view projection while maintaining sharpness and low geometric and photometric distortions.*

## 1. Introduction

The recent introduction and rapid adoption of consumer digital projectors has redefined the landscape for displaying images and videos. To model projection geometry, a projector is commonly treated as a virtual pinhole camera and classical perspective geometry can then be directly applied to analyze the projection process [20]. Recent developments in camera designs have suggested alternative non-pinhole cameras [11, 8] that can capture potentially advantageous images. This gives rise to the question whether we can design non-pinhole-based projection systems.

In this paper, we present a new class of projection systems called catadioptric projectors. Our work is inspired by the catadioptric cameras [1, 2, 5, 9, 11, 12, 19, 24] that place a pinhole camera in front of curved mirrors or refractors. We show that by combining a commodity digital projector with similar optical units, the catadioptric projector can offer an unprecedented level of flexibility in aspect ratio, size, and field of view (Figure 1). Our catadioptric projectors assume unknown reflector/refractor geometry and do not require accurate alignment between the projector and the optical units. In fact, we use everyday reflective and refractive objects such as plastic mirrors, security domes, and even wine glasses.

The complex geometry of the reflective and refractive objects can cause severe distortions, scattering, and defocusing. In this paper, we propose several new algorithms to effectively reduce these artifacts without recovering the reflector/refractor geometry. Our approach directly models the light transport between the projector and the viewpoint using the light transport matrix (LTM). We show that every two rows of the LTM from the projector to the viewpoint are nearly orthogonal. We then develop a simple method to approximate the pseudo inverse of the LTM and apply it to find the optimal input image that produces least projection distortions.

Finally, we present a projection defocus analysis for mirror and thin refractor-based catadioptric projectors. We show that defocus blur can be interpreted as spatially-varying Gaussian blurs on the input image. We then measure the kernels directly from the LTM and apply deconvolution to optimize the input image. We demonstrate the practical uses of catadioptric projectors in panoramic and omni-directional projections. Our new system achieves much wider field-of-view projection while maintaining sharpness and low geometric and photometric distortions.

## 2. Related Work

**Projection System.** High resolution and high contrast projectors are increasingly used in a wide array of commercial and scientific applications, ranging from shape acquisition [27], to virtual environments [16, 7] and IMax theaters

978-1-4244-3991-1/09/$25.00 ©2009 IEEE 

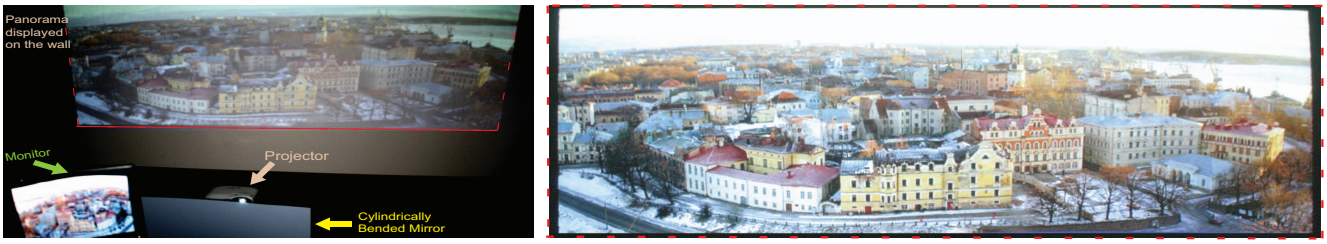


Figure 1. Left: A panoramic catadioptric projector that combines a regular projector with curved plastic mirror. Right: The final projection uses the the projector's full resolution ($1024 \times 768$) and is displayed on a $16m \times 3m$ wall.

[10]. In vision and graphics applications, cameras are often combined with projectors to form a projector-camera or ProCam system, for creating intelligent projections. The pioneering works [16] put forth the vision of intelligent projection systems serving as novel tools for problem solving. Using pre-authored 3D models of the objects, shader lamps [15] can add virtual texture and animation to real physical objects with non-trivial complicated shapes. It is also possible to use space-time-multiplexed illumination in a ProCam system to recover scene depth [27].

Like pinhole cameras, a projector suffers from limited field-of-view, e.g., it would be difficult to produce a panoramic projection using a single projector. One possible solution is to use multiple projectors and significant advances have been made in automatic mosaicing of multiple projectors [6, 26, 20, 14]. However, these systems require accurate geometric and photometric calibration between the projectors. In this paper, we present an omni-directional projection system that only uses a single projector.

**Catadioptric Cameras.** Our work is inspired by catadioptric camera designs that place a virtual pinhole camera in front of specially shaped mirrors or reflectors to synthesize a wider field of view. Classical examples include single viewpoint catadioptric sensors based on hyperbolic or parabolic mirrors [25, 11, 1, 13] and multiple viewpoint sensors based on spherical, conical, and equiangular mirrors [24, 2, 3, 5]. Catadioptric cameras have also been used to capture high resolution 360 degree [12] or cylindrical panoramas [9, 19]. Most of these systems require accurate alignment of the viewing camera. When the camera moves off the focus, the reflection rays form complex caustic surfaces that are difficult to analyze [21].

In this paper, we present a catadioptric projector that combines a commodity projector with similar optical units used in catadioptric cameras. The key difference, however, is that we do not require knowing or recovering reflector/refractor geometry. Instead, we seek to, given a projector and a viewpoint, compute the image the projector should use to illuminate the scene for that specific viewpoint. We address the problem by studying how light propagates between the projector and the desired viewpoint.

**Light Transport.** Modeling light transport through a known 3D environment is a well-studied problem in computer graphics. Consider emitting unit radiance along ray $i$ towards the scene. The ray can be reflected, refracted, scattered, or simply pass through the scene. We can then capture the full transport $t_i$ in response to the impulse illumination of $i$. $t_i$ is often referred to as the impulse scatter function or ISF. We can measure the light transport for each incident ray and concatenate all ISF into a light transport matrix or LTM $T$. If we represent the incident illumination as $L_{in}$, then the outgoing light field can be expressed as a function of the illumination by $L_{out} = TL_{in}$.

To measure $T$, one can emit a 2D incident light field (an image) $L_{in}$ using a projector and capture the 2D/4D outgoing light fields using a camera or a camera array. [18] showed that by the principle of Helmholtz reciprocity, the light transport can be used to model a 'dual' setup where the projector is replaced by a virtual camera and the camera by a virtual projector. This enables *Dual Photography*, where one can *synthesize* images that appear as though they were captured by the projector, with the scene illuminated by light emitting from the camera.

Our goal is to find the input image to the catadioptric projector that when used to illuminate the scene, allows the camera to *capture* a given desired view. This is a typical inverse light transport problem. Seitz et. al. derived the closed-form expression for computing the inverse LTM in the Lambertian environment [17]. Wetzstein et. al. used inverse LTM to perform radiometric compensation in projection. For non-Lambertian environments such as the ones we use in our catadioptric projector setup, it remains an open problem on how to effectively approximate the inverse LTM.

## 3. Catadioptric Projector Designs

A catadioptric projector combines a commodity digital projector with additional optical units. It follows similar design principles in catadioptric cameras: we choose specially shaped mirrors for synthesizing a wider field-of-view. However, it differs from catadioptric cameras in several ways.

**Mirror Shape and Size.** In catadioptric cameras, it is often sufficient to use mirrors of approximately the same size as the lens ($\leq$ 5cm in diameter) to synthesize the desired field-of-view. However, a projector uses a much bigger lens and has a longer focal length. Therefore, it is nec-

essary to use custom built larger sized mirrors ($\geq$ 20cm in diameter) to produce panoramic projections. In our setup, we simply bend a plastic mirror to approximate a cylindric mirror (Figure 1(a)) and use a security dome to approximate a spherical mirror (Figure 6(a)). We even use wine glasses to emulate thin refractors (Figure 8(a)). However, these surfaces are not perfectly polished and usually have micro-structures such as bumps and dimples that can lead to geometric distortion, scattering, and blurring.

**Physical Setup.** Catadioptric projectors differ from catadioptric cameras in the physical setup. In a catadioptric camera, the physical camera needs to be accurately positioned at the focus of a hyperbolic or parabolic surface to synthesize a virtual pinhole camera. The physical camera itself, hence, will occupy the center part of the captured image. This does not cause much problem for catadioptric imaging as its goal is to capture the surrounding environment and the center portion of the image can be discarded, especially if the physical camera is small. However, similar setups can cause severe self-shadowing. Therefore, in our setup, we purposely move the projector away from the focus of the mirror and orient the projector so that it will not block the light path.

**Defocus Blur.** Defocusing artifacts are more severe in catadioptric projectors than in catadioptric cameras. Most catadioptric cameras use a small aperture to increase the depth-of-field while projectors have to use large apertures to produce bright images. Furthermore, since the virtual projector of a catadioptric projector has multiple COPs while the physical projector can only set a uniform focal length, the final projection will exhibit spatially-varying defocus blurs.

To resolve these challenges, we first present novel algorithms for correcting projection distortions by modeling the light transport matrix between the projector and camera (Section 4). We then analyze the defocus model in catadioptric projectors and develop effective methods to minimize the defocus blur by pre-processing the input image (Section 5). In Section 6, we demonstrate several applications of our system.

## 4. Correcting Geometric and Photometric Distortions

Given a catadioptric projector and a viewpoint represented by a camera, we seek to find the optimal image to be displayed by the projector so that it will be viewed with minimum geometric and photometric distortions from the camera.

### 4.1. Light Transports in Catadioptric Projectors

Assume the projector has a $m$-row-by-$n$-column imaging element while the camera has a $s$-row-by-$t$-column sensor, as shown in Figure 2. Light rays emitting from the projector bounce off the scene and some of them eventually reach the sensor. In general, each ray of light is dispersed, reflected, and refracted in the scene and hits the camera sensor at a number of different locations. Thus the light ray passing through pixel $i$ in the projector reaches the camera and forms an $s$-by-$t$ image, where each pixel $j$ receives a certain amount of light. If we represent the image projected as a $m \times n$-element vector $p$ and the image captured as an $s \times t$-element vector $c$, then the light transport between the projector and camera can be written as

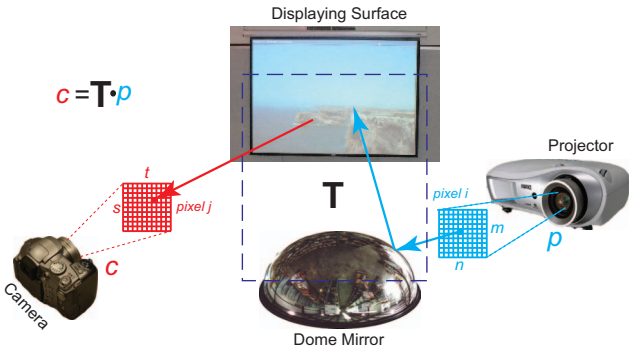


Figure 2. Light transport in a catadioptric projector: lights emitted from the projector are reflected or refracted before reaching the screen. The light transport matrix $T$ correlates each projector pixel to a camera image.

$$c = Tp$$

where $T$ is the light transport matrix.

Our goal is to solve the inverse light transport problem, i.e., given the desired view $c$ and the LTM $T$, what should be the source image $p$. Intuitively, $p$ can be found with

$$p = T^{-1}c$$

provided we can find $T^{-1}$. Thus, we aim to compute the inverse of the LTM $T$ of the camera-projector pair. However, the sheer size of $T$ makes computing $T^{-1}$ an extremely challenging task requiring tremendous computational resources, e.g., we used a camera of 3072x2304 pixels and the projector of 1024x768 pixels. Thus, T's dimension is 3072x2304 by 1024x768. Moreover, it is not always possible to find the inverse of an arbitrary matrix. Fortunately, as we show below, for most settings that we are interested in, it is possible to find an approximation for $T^{-1}$ that can be efficiently computed.

### 4.2. Fast Approximation for $T^{-1}$

Recall that in a typical projector-camera setup, any two distinct light rays $j$ and $k$ emitting from the projector will typically hit distinct regions of the camera sensor, i.e., there is usually little overlap in the camera sensor pixels hit by light from each of the rays. We call this the *display constraint*. Furthermore, since each column of the transport

matrix $T$ is the projection image of one pixel from the projector. This implies that most column entries have zero values except those corresponding to the camera pixels hit by light emitting from the corresponding projector pixel.

By the display constraint, light from different projector pixels will mostly hit different camera pixels. This means that if two columns of $T$ are placed next to each other, the non-zero entries will not line up most of the time, and their dot product will be close to zero. This implies that the columns of $T$ are *orthogonal* to each other. Therefore, to find an approximation to $T^{-1}$, we can construct a matrix $\tilde{T}$ such that

$$\tilde{T}_i = T_i / (\| T_i \|)^2, i = 1, \ldots, pq \quad (1)$$

where $\tilde{T}_i$ is the $i_{th}$ column of $\tilde{T}$. Since

$$\tilde{T}_i^T T_i = 1 \quad \text{and} \quad \tilde{T}_i^T T_j = 0, i \neq j$$

This means that

$$\tilde{T}^T \approx T^{-1} \quad \text{and} \quad p \approx \tilde{T}^T c.$$

Note that our approximation to the inverse LTM can only applied to the projector pixels whose light emitted actually reaches the camera sensor. For the projector pixels whose light never reach any of the camera pixels, the corresponding columns in $T$ will be all zeros and Equation (1) is undefined. In these cases we simply set the corresponding columns in $\tilde{T}$ as zero columns. Thus $\tilde{T}^T$ is the inverse of the part of $T$ that covers the overlapping area of the fields-of-views (FOV) of the projector and the camera. It only recovers the projector pixels in $p$ that fall in the overlapping FOV and blacks out the other pixels. Once we compute $\tilde{T}^T$, we can directly apply it to the target image $I$ to find the optimal input image. $\tilde{T}^T$ is also referred to as the View Projection Matrix and has been used in other projection applications such as multi-projector mosaicing and virtual projection [22].

### 4.3. Acquisition and Results

To acquire $T$, we adopt the approach in [22]. It lightens up only one row or one column of the projector image at a time with a white color of intensity 255. The projected one-row or one-column images are captured by the camera individually. The common non-ambient pixels of the $i_{th}$ row image and the $j_{th}$ column image are brightened by the projector pixel $(i, j)$. The coordinates of these pixels determine the indices of the non-zero values in the column of $T$ corresponding to the projector pixel $(i, j)$, and the actual non-zero $T$ values are acquired as the average colors of these individual pixels over the two images. This process goes through all pairs of one-row and one-column images and $T$ is entirely acquired.

The dome catadioptric projector consists of a nearly spherical mirror and a regular commodity projector. Without inverse LTM correction, we observe severe geometric distortions such as stretching and shearing of the patterns in the final projection (Figure 7). Unlike an ideal spherical mirror, the geometric distortions caused by the dome are nonuniform due to the micro-structures on the mirror such as bumps and dimples. They also introduce additional photometric distortions like inter-reflection. Finally, as the mirror we use is not perfectly specular, we observe that the center of the projection is brighter than the boundary. Nevertheless, using the inverse LTM approximated by our approach, we are able to significantly reduce both the geometric and photometric distortions as shown in Figure 7.

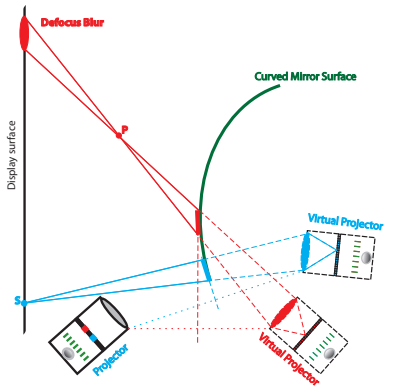


Figure 3. We can decompose a curved mirror into piecewise linear patches and map the physical projector a virtual projector for each patch. This results in spatially-varying projection defocus.

In general, the display constraints may be violated if there is significant scatter in the scene, for example in the reflector experiment shown in Figure 8. In Figure 8, we project "CVPR 09" pattern through two thin wine glasses. The final projection exhibits more severe photometric distortions than geometric distortions, e.g., scattering artifacts around the boundaries of the glasses. Furthermore, since the refracted rays form caustics, we observe uneven brightness across the displayed image. Since both scattering and caustics are captured by the LTM, we are able to significantly reduce all these artifacts using the approximated LTM as shown in Figure 8.

Our approach, however, cannot compensate for shadows caused by occlusions. Notice that near the occlusion boundaries of the glasses, the incident rays reach the grazing angle. The transparent glasses hence behave like opaque objects near the boundary and cast shadows on the final projection. In the future, we plan to explore combining multiple projectors to remove the shadows.

## 5. Defocus Compensation

Our light transport model assumes that each pixel from the projector is a single ray. This corresponds to the small aperture model for cameras. In practice, projectors use large apertures to produce bright images and multiple light rays pass through the same projector pixel. In theory, we should

use the 4D incident light field rather than the 2D image to model the LTM. Therefore, our inverse LTM cannot correct visual artifacts caused by the 4D incident light field, e.g., project defocus [27, 4].

In this section, we present a simple solution for modeling projection defocusing. We assume projection blur can be equivalently interpreted as to first blur the input image by the blur kernel $G$ and then transported by the LTM $T$. We will validate this model in both the reflection and refraction cases. The final light transport from the projector the camera be then written as:

$$c = T^* \cdot p = T \cdot G \cdot p \tag{2}$$

where $T^*$ is our captured LTM, $G$ is the blur matrix, and $T$ is the LTM based on a small aperture. The optimal input image $p$, hence, can be computed as:

$$p = T^{*-1} \cdot c = G^{-1} \cdot T^{-1} \cdot c \tag{3}$$

To compute $T^{-1}$, recall that the display constraint is still satisfied if we apply $G^{-1}$ on $T^{-1}$. Therefore, we can simply apply the inverse LTM algorithm on the captured $T^*$ to obtain $T^{-1}$. Next, we show how to compute $G^{-1}$.

### 5.1. Reflector Case

We start by analyzing the cause of projection defocus in reflector-based catadioptric projectors as shown in Figure 3. Given a curved mirror and a projector, we can first approximate the mirror as piecewise linear (PL) surfaces. For each planar patch, we map the physical projector to a virtual projector using the reflection geometry. The catadioptric projector, hence, can be treated as a loci of virtual pinhole projectors.

If we use specially shaped reflectors such as hyperbolic or parabolic mirrors and position the physical projector at the focus, all virtual projectors will lie at the same COP. To minimize projection defocus, we can simply set the focal plane of the virtual projector close to the display screen. For general mirrors, the loci of the virtual projectors correspond to complex caustic surfaces [21]. This implies that the virtual projectors will lie at different depths with respect to the display screen. Since the physical projector can only have a single focus, the virtual projectors will produce spatially-varying projection blurs, as shown in Figure 5. Since each virtual projector can be viewed as a camera, projection defocus hence can be treated as circle-of-confusion of virtual cameras, as shown in Figure 3. In our setup, we assume the reflector is highly smooth and the projection screen is nearly parallel to the image plane of the virtual projectors. Therefore, we can simply use spatially-variant Gaussian blurs to approximate the blur kernels.

To acquire the kernel size, one can project dotted patterns and capture their defocused images [27]. Notice this

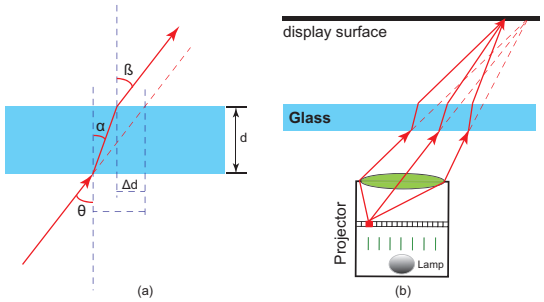


Figure 4. Catadioptric Projectors Using Thin Refractors. (a) A ray is shifted by the thin refractor. (b) The focus of the projector is also shifted if the refractor is thin.

is very similar to our LTM acquisition process. However, the non-zero terms in the LTM are a mixture of projection defocus and light transport (e.g., inter-reflections). For curved mirrors, we assume these non-zero terms are dominantly caused by defocus. Therefore, we simply reuse the captured LTM $T^*$ for estimating the blur kernels: we compute, for every projector pixel $(i, j)$, the non-zero terms in its corresponding column in the LTM $T^*$ and then fit a 2D Gaussian kernel $g_{i,j}$ to these pixels. Once we obtain the defocus kernel $G$ and the inverse LTM $T^{-1}$, we first multiply $T^{-1}$ to the target image $c$ and then apply deconvolution on the result image using kernel $G$. In our implementation, we adopt the steepest descent approach used in [27].

### 5.2. Thin Refractor Case

Next, we consider projection defocus in catadioptric projectors that use thin layer(s) of transparent surfaces. A typical example is projecting through the wine glasses as shown in Figure 8.

To study defocusing, we first analyze how rays propagate through the refractor as shown in Figure 4. Assume $d$ and $m$ represent the thickness and the refractive index of the glass. For a each ray with incident angle $\theta$, it will first pass through the front face and then leave the back face. Let $\alpha$ and $\beta$ represent the front and back exiting angle. Assuming the medium on both sides of the refractor is the same, then using Snell's Law, we have

$$\frac{\sin\theta}{\sin\alpha} = m, \qquad \frac{\sin\alpha}{\sin\beta} = \frac{1}{m} \tag{4}$$

Thus, we must have $\theta = \beta$, i.e., the exit direction of a ray will be the same as its incident direction to the front face of the refractor. The exit ray, however, is slightly shifted by $\Delta d$, where

$$\Delta d = d\tan\theta - d\tan\alpha = d(\tan\theta - \frac{\sin\theta}{\sqrt{m^2 - \sin^2\theta}}) \tag{5}$$

If we assume the projector is placed relatively far away from the display screen, then all the rays that originate from an image pixel $p$ from the projector will have approximately the same incident direction $\theta$. The refraction equation (5) shows that these rays will be uniformly shifted after passing

through the thin refractor. Therefore, since the incident rays focus at a 3D point if not refracted, their new focus will simply shift by $\Delta d$ from the old focus. If we assume the refractor is nearly parallel to the display screen, the new focus will still lie on the display screen, as shown in Figure 4. This implies that projection defocus is negligible for thin refractors as shown in Figure 4.

Recall that upon exiting the back face of the refractor, some portion of the ray will also be reflected back into the refractor. This leads to the scattering artifacts when projecting through thin refractors. The scattering, however, is captured by the LTM and can be effectively corrected using our inverse LTM-based correction algorithm. In the case of thin wine glasses, we can simply repeat our analysis on single-layered thin refractors to model both layers. Scattering artifacts, however, will be more severe when projecting through multiple layers. Our inverse LTM-based approach is able to effectively reduce these artifacts as shown in Figure 9.

## 6. Results

In this section, we demonstrate using our catadioptric projection systems for displaying panoramic and omnidirectional images.

**Panoramic Projection.** Capturing and synthesizing panoramic views of complex scenes have attracted much attention in computer graphics and vision [13, 12]. However, very little work has been done to effectively display these panoramic images. The main difficulty lies in the limited aspect ratio of the projectors. For example, it is common for panoramas to have an aspect ratio of 3:1 while a commodity projector can achieve at most a 1.2:1 aspect ratio. A simple solution is to enforce the same aspect ratio in the projected image (e.g., by displaying a $1024 \times 200$ image). However, it will waste a large amount of the resolution. Furthermore, since a projector usually has a narrow field-of-view, it is difficult to display the panorama on a wide area.

In our system, we combine a commodity projector (Epson PowerLite 78 projector with resolution $1024 \times 768$) with a cylindrical mirror. Instead of using custom designed mirrors, we simply use a 10-dollar plastic mirror. We bend the mirror to near cylindrical shape and place it in front of the projector, as shown in Figure 1. The resulting projection can achieve an aspect ratio of 3:1 and the projected source image uses the maximum resolution of the projector as shown in Figure 1. It is also interesting to note that the geometry of the mirror makes our projector a virtual pushbroom projector [8]. Although the horizontal direction has a much lower resolution than the vertical direction, we find that the high vertical resolution can often effectively compensate for the low horizontal resolution.

**Omni-Directional Projection.** Developing inexpensive solutions for creating omni-direction projection effects similar to IMAX at home or school can significantly benefit education, scientific visualization, and digital entertainment. However, the difficulty lies in several aspects. First, IMAX projectors use fisheye lenses to simulate 180 degree projection whereas most commodity projectors use regular lenses and have a much smaller field-of-view. Second, although it is possible to combine multiple projectors to synthesize omni-directional projections, robust and efficient calibration between the projectors is still an open problem. Finally, IMAX systems use dome-shaped projection screens whereas regular rooms at home or school are rectangular shaped.

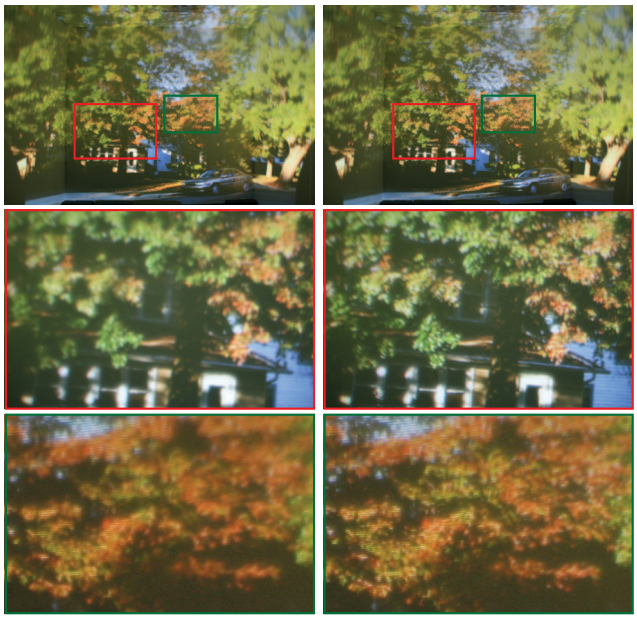

Figure 5. Defocus Compensation Results Using the Dome Projector. Left row shows the inverse LTM results without defocus compensation. Right row shows the results by applying defocus compensation on the inverse LTM corrected images.

Here we synthesize an omnidirectional projection system by combining a commodity projector with a security dome. We place a reflective security dome in front of the projector and orient the projector so that it will not block the final projection after reflection. The dome has a radius of 20cm and we position the projector approximately 30cm away from the dome. This creates an approximately 180 degree field-of-view of the final projection.

We conduct our experiment in a room of $4m \times 6m \times 3m$ and the dome is positioned about 0.5m from the front wall. The reflected projection becomes omnidirectional by covering the four sides of the wall, as shown in Figure 6. However, unlike an IMAX dome, the different orientations of the walls cause projection discontinuities, as shown in 7. Furthermore, we observe strong geometric distortions and non-uniform angular resolutions due to the geometry of the sphere. Finally, the direct use of our setup also suffers from micro-structures of the geometry. In fact, we find, through


Figure 6. Omni-directional Projection Using a Dome Projector. (a) and (c) show the projection results before applying distortion correction. (b) and (d) show the results by applying the inverse LTM and projection defocus compensation.

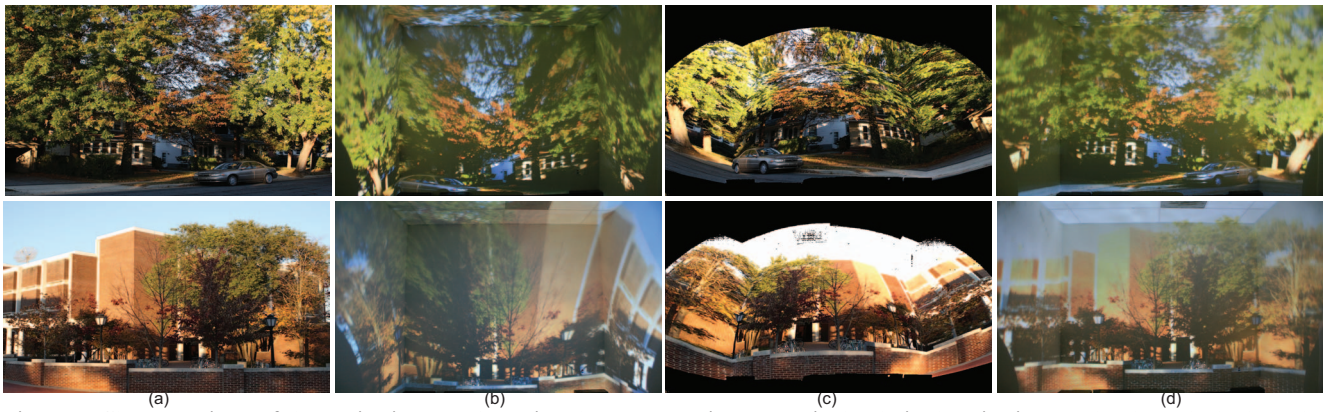


Figure 7. Close-up Views of the Projection Results Using the Dome Projector. (a) is the desired projection result. (b) and (d) show the projection results before and after distortion and defocus compensation. (c) show the actual images that are projected.

our experiment, that the dome is far from being perfectly spherical: there are many micro-structures such as bumps and dimples. However, our inverse LTM-based algorithm can effectively correct most of the distortions and our deconvolution method improves non-uniform projection defocus blur as shown in Figure 5.

## 7. Conclusions and Future Work

We have presented a catadioptric projector analogous to a catadioptric camera by combining a commodity digital projector with additional optical units. Our system does not require recovering the reflector/refractor geometry. In fact, our setup uses everyday objects such as plastic mirrors and wine glasses, whose geometry is difficult to recover. Our approach models the light transport between the projector and the viewpoint using the light transport matrix (LTM). We have shown how to efficiently approximate the pseudo inverse LTM and use it to find the optimal input image that will incur minimum distortion. Furthermore, we have also presented a projection defocus analysis for catadioptric projectors. We interpret the defocus blur as spatially-varying Gaussian blurs, where the kernels can be directly measured from the LTM. We have then applied deconvolution techniques to pre-process the input image to minimize the defocus blur in the final projection. We have demonstrated the practical uses of catadioptric projectors in panoramic and omni-directional projections. We have shown that, by using specially shaped reflectors/refractors, catadioptric projectors can offer an unprecedented level of flexibility in aspect ratio, size, and field-of-view while maintaining sharpness and low geometric and photometric distortions.

A major limitation of our approach is that we cannot separate defocus blur from the actual light transport in the captured LTM. For reflectors and thin refractors, either the defocus blur or the scattering will dominate the non-zero terms in the LTM, and thus, they can be separated. However, for more general reflectors or refractors such as thick refractors, the captured LTM is a mixture of blurs and transport. In the future, we plan to develop effective acquisition methods for separating the two terms using coded patterns. It may also be possible to use our LTM-based framework to recover the specular geometry, e.g., by using path tracing. Finally, we plan to develop real-time distortion and defocusing compensation methods for displaying panoramic videos using our projectors. We hope that catadioptric projectors will serve as conceptual inspiration for designing new generations of projection systems.

**Acknowledgement**
This work was initialized and developed in Epson R&D Inc., Yuanyuan Ding and Jingyi Yu were partially supported by the National Science Foundation under grant NSF-MSPA-MCS-0625931.

## References

[1] S. Baker and S.K. Nayar, 1998. A theory of catadioptric image formation. In Proc. ICCV, pp. 35–42.

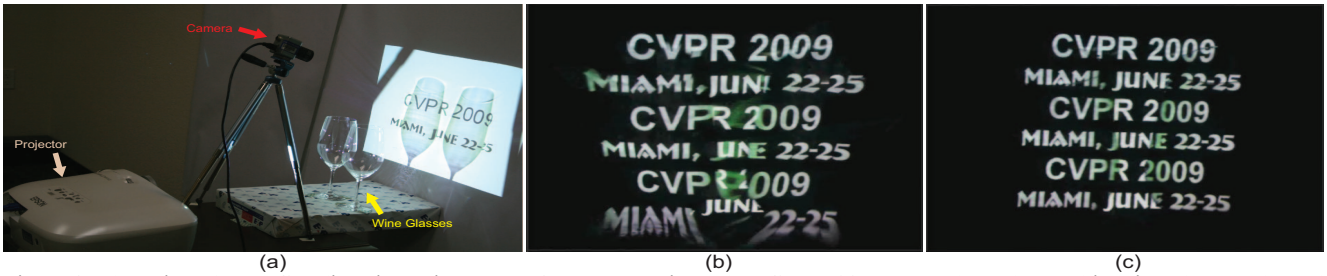


(a) (b) (c)

Figure 8. The Wine-glasses Catadioptric Projector. (a) Our setup projects the "CVPR 09" pattern through two thin wine glasses. (b) and (c) show the projection results before and after the inverse LTM correction.

(a) (b) (c) (d)

Figure 9. Close-up Views of the Wine-glasses Projector Results. (a) is the desired projection result. (b) and (c) show the projection results before and after distortion correction. (d) shows the actual projected image.


[2] S. Bogner, 1995. Introduction to panoramic imaging. In IEEE SMC Conference, vol. 54, pp. 3100–3106.

[3] R.C. Bolles, K.G. Konolige, and M.A. Fischler, 1997. Extra set of eyes. In DARPA-IUW, pp. 41–44.

[4] M. S. Brown, P. Song, and T.J. Cham, Image Preconditioning for Out-of-Focus Projector Blur, Computer Vision and Pattern Recognition (CVPR06), June 2006

[5] J. Chahl and M. Srinivasan. Reflective surfaces for panoramic imaging. Applied Optics 1997.

[6] H. Chen, R. Sukthankar, G. Wallace, and K. Li. Scalable alignment of large-format multi-projector displays using camera homography trees. In Proceedings of IEEE Visualization, 2002.

[7] K. Fujii, M. D. Grossberg, and S. K. Nayar. A projector-camera system with real-time photometric adaptation for dynamic environments. In Proceedings IEEE CVPR, 2005.

[8] R. Gupta and R.I. Hartley: Linear Pushbroom Cameras. IEEE Trans. Pattern Analysis and Machine Intelligence, vol. 19, no. 9 (1997) 963–975.

[9] R. Hicks, and R. Perline, 2002. Equi-areal catadioptric sensors. In Proc. OMNIVIS, p. 13.

[10] E. Lantz, A survey of large-scale immersive displays. In: EDT '07: Proceedings of the 2007 workshop on Emerging displays technologies, p. 1 (2007)

[11] S.K. Nayar, 1997. Catadioptric omnidirectional cameras. In Proc. CVPR, pp. 482–488.

[12] S.K. Nayar, and A.D. Karmarkar, 2000. 360 360 Mosaics. In Proc. CVPR, pp. I:388–395.

[13] V.N. Peri and S.K. Nayar 1997. Generation of perspective and panoramic video from omnidirectional video. DARPA-IUW, pp. I:243–245.

[14] R. Raskar, J. van Baar, P. Beardsley, T. Willwacher, S. Rao, and C. Forlines. ilamps: Geometrically aware and self-configuring projectors. In ACM SIGGRAPH, 2003.

[15] R. Raskar, G. Welch, K. lim Low, and D. Bandyopadhyay. Shader lamps: Animating real objects with image-based illumination. In Proceedings 12th Eurographics Workshop on Rendering, 2001.

[16] R. Raskar, G.Welch, M. Cutts, A. Lake, L. Stesin, and H. Fuchs. The office of the future: A unified approach to image-based modeling and spatially immersive displays. In Proceedings ACM SIGGRAPH, 1998.

[17] S. M. Seitz, Y. Matsushita, and K. N. Kutulakos. A theory of inverse light transport. In Proceedings IEEE ICCV, 2005.

[18] P. Sen, B. Chen, G. Garg, S. R. Marschner, M. Horowitz, M. Levoy, and H. P. A. Lensch. Dual photography. In Proceedings ACM SIGGRAPH, 2005.

[19] M. Srinivasan, 2003. New class of mirrors for wide-angle imaging. In Proc. OMNIVIS.

[20] R. Sukthankar, R. G. Stockton, and M. D. Mullin. Smarter presentations: Exploiting homography in camera-projector systems. In Proceedings IEEE CVPR, 2001.

[21] R. Swaminathan, M. D. Grossberg, and S. K. Nayar. Nonsingle viewpoint catadioptric cameras: Geometry and analysis. IJCV, 66(3):211C229, 2006.

[22] K.-H. Tan, J. Xiao, A. K. Bhattacharjya, Efficient Dual Photography, Invention Disclosure, Epson R&D, Inc., 2006.

[23] G. Wetzstein and O. Bimber, "Radiometric Compensation through Inverse Light Transport," pg,pp.391-399, Pacific Graphics '07

[24] Y. Yagi, S. Kawato, and S. Tsuji, 1994. Real-time omnidirectional image sensor (copis) for vision-guided navigation. Robotics and Automation, 10(1):11–22.

[25] K. Yamazawa, Y. Yagi, and M. Yachida, 1993, Omnidirectional imaging with hyperboloidal projection. In Proc. IEEE/RSJ International Conference on Intelligent Robots and Systems, pp. 1029–1034.

[26] R. Yang, D. Gotz, J. Hensley, H. Towles, and M. S. Brown. Pixelflex: A reconfigurable multi-projector display screen. In Proceedings IEEE Visualization, 2001.

[27] L. Zhang, S. Nayar. Projection defocus analysis for scene capture and image display. In: ACM SIGGRAPH 2006 Papers, pp. 907–915 (2006)